Influence of surface topography on torsional fretting wear under flat-on-flat contact

Wenlong Lu[1], Po Zhang[1,*], Xiaojun Liu[1],Wenzheng Zhai[1],Mingzhuo Zhou[1],Jian Luo[1],Wenhan Zeng[2],Xiangqian Jiang[2]

[1]*The State Key Laboratory of Digital Manufacturing Equipment and Technology, School of Mechanical Science and Engineering, Huazhong University of Science and Technology, Wuhan 430074, PR China*

[2]*EPSRC Centre for Innovative Manufacturing in Advanced Metrology, University of Huddersfield, Huddersfield, HD1 3DH, UK*

Abstract: Influence of surface topography on torsional fretting under flat-on-flat contact were investigated. Contact surfaces of the lower specimens were prepared by milling with different initial surface roughness while the upper specimens were polished. Results indicate that with the increase of surface roughness, friction torque and accumulated dissipated energy present a first increase and then decrease tendency and are higher when the texture is perpendicular to the relative movement direction. The wear volume and wear rate present increasing and decreasing tendencies separately for textures parallel and perpendicular to the relative movement direction, and they are higher when the texture is parallel to the relative movement direction. The results can provide guidance for the initial surface design to reduce fretting wear.

Keywords: surface roughness; texture direction; torsional fretting; friction and wear

1. Introduction

Surface topography is the local deviation of a surface from a perfectly flat plane, and it has become increasingly important in many fields, such as materials, tribology and machine condition monitoring [1-2]. In many industrial applications the fretting degradation process is inevitable. After investigation, it has been concluded that surface topography can have a great influence on the fretting wear behavior [3-7]. It is therefore very important to understand how surface topography correlates with fretting wear behavior, so that initial design can be optimized to prevent or reduce the fretting phenomenon and surface damage.

Most previous research on relation between surface morphology and friction behavior has focused on mono-directional sliding or sliding under gross slip conditions [8-11]. Krzysztof J Kubiak et al. investigated the influence of surface topography on the wear and friction behavior under tangential fretting with the ball-on-flat contact configuration [12-16]. However, in many engineering applications, the fretting mode is not tangential and the contact configuration is also not ball-on-flat. For example, fretting between the hub and the blade carrier in a controllable pitch propeller, and fretting between the bogie and the railcar body on

a train are all typical torsional fretting under flat-on-flat contact [17-19]. Both the fretting modes and contact form have a great influence on the fretting wear behavior. Previous studies done by ZB Cai et al. have revealed that both the running behavior and wear mechanisms are different under different fretting modes (four basic fretting modes: tangential, radial, rotational, torsional) [20-21]. The contact form can also be crucial, as with the same normal load and same materials but different contact forms the contact stress distribution, contact stiffness and the action of the wear debris differ greatly [22-23].

In this study, experimental tests are carried out with a torsional fretting wear device with flat-on-flat contact. The fretting wear behaviors such as friction torque and wear rate are examined under different surface roughness and different texture directions. By finding a correlation between the surface topography and torsional fretting wear properties, a reliable procedure for the optimization of the processing techniques to improve the wear-resisting property of the surface can be drawn up.

2. Experimental details

2.1. Test rig and materials

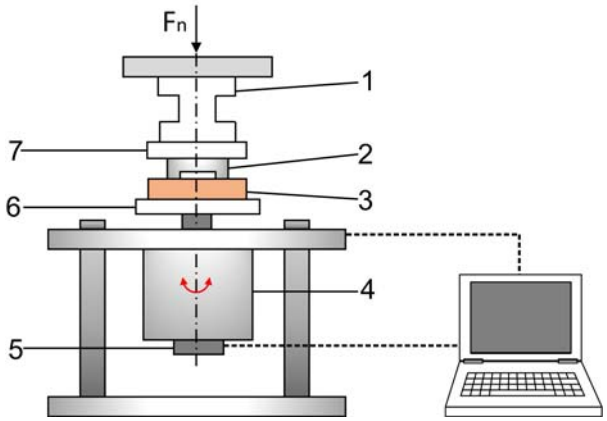

Fig. 1. Schematic of torsional fretting wear test rig for flat-on-flat configuration. (1) Torque sensor; (2) Upper specimen; (3) Lower specimen; (4) Stepping motor; (5) Encoder; (6) Lower holder; (7) Upper holder

The experimental tests were performed on a torsional fretting test rig with a flat-on-flat contact configuration, as schematically shown in Fig. 1. The lower holder was driven by a reduced speed stepping motor (Model: 57PG1440-010; Step angle accuracy 0.018; Maximum output torque 6N.m; Speed range 0-120r/min). Angular displacement amplitude of the fretting test (setting range, 0.1° to 3°) was controlled by the impulse number in a fretting cycle; frequency of the fretting test (setting range, 1Hz to 3Hz) was controlled by the motor impulse frequency. The lower specimen was fixed on the lower holder and rotated following the motion of the stepping motor. The upper specimen was fixed on the upper holder, which was

connected to a torque sensor (Model: TJN-3; Test range: -2.5Nm to +2.5Nm; Combined error: ≤ 0.5% F·S). Centerline alignment of the upper specimen and lower specimen was guaranteed by careful mechanical design and adjustment. Normal loads (P) were applied by dead weights from the top. The angular displacement amplitude (θ) of the contact interface were measured by an encoder, which is mounted at the end of the stepping motor.

Investigation done by Godjevac M et al. revealed that blade bearings are key components for a controllable pitch propeller, but fretting between the hub and blade carrier lead to the wear failure of the blade bearing [17]. 42CrMo4 ((wt %) 0.38-0.45C, ≤0.40Si, 0.60-0.90Mn, 0.035P, ≤0.035s, 0.90-1.20Cr, 0.15-0.30Mo) is the typical material used for the blade carrier; CuNiAl ((wt %) 9.0-9.5Al, ≤0.1Si, 0.8-1.3Mn, 4.5-5.1Fe, 4.2-4.8Ni, 78.5-80.5Cu, 1.5-3.5Zn, ≤0.1Sn, ≤0.03Pb) is the typical material used for the hub. In this study, 42CrMo4 and CuNiAl are selected for the upper and lower specimens respectively. Their physical and mechanical properties are shown in Tables 1.

Table 1
Mechanical properties for the friction pair.

Material	Yield strength σ_s(MPa)	Tensile strength σ_b (MPa)	Elasticity modulus E (MPa)	Poisson's ratio υ	Hardness(HB)
CuNiAl	250	650	121,000	0.33	127
42CrMo4	550	800	212,000	0.3	220

The experimental parameters were set according to the practical operating condition of the blade bearing [17]: the normal load was kept constant at P=86N; the frequency was set at 2Hz; the angular displacement was 1.5° and the test duration was 40,000 cycles. Tests were performed at 23°C in laboratory ambient conditions and at 40-45% relative humidity. Before testing, all specimens were ultrasonically cleansed in acetone and ethanol in turn to remove the organic contaminant. Finally, they were dried in a well-ventilated area with hot compressed air.

2.2. Preparation of test specimens

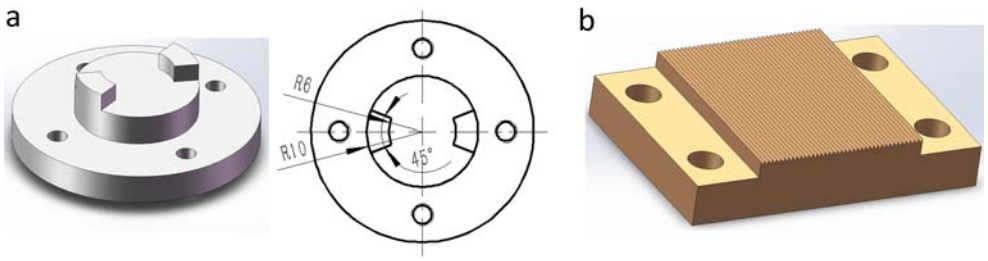

Fig. 2. Specimens used for the fretting wear tests. (a) Upper specimen designed with two 45°, sectors of a raised ring; (b) Lower specimen designed with textured contact surface;

The macro geometrical configuration of the specimen design is shown in Fig. 2. The upper specimen was designed with two raised 45° sectors of a ring. Having the specimens contact at two ring sectors has a number of advantages over a full disk-to-disk contact: reducing the surface area allows testing over a larger range of pressures; separating the steps by the ring diameter stabilizes the contact and prevents tipping; decreasing the contact area reduces the surface area and increases the depth of a wear scar so wear volume can be measured more accurately [22].

Table 2
Machining parameter and corresponding initial surface roughness.

Surface reference	Machining parameters		Surface roughness S_a/μm
	Rotation rate	Feed rate	
Surface.1	750	75	1.737
Surface.2	600	95	2.816
Surface.3	600	115	3.155
Surface.4	475	115	3.219
Surface.5	375	95	4.299
Surface.6	375	115	4.553
Surface.7	300	115	5.261

During the preparation of the specimens, the contact surfaces of the upper specimens were all polished to the roughness of 0.05μm, while the contact surfaces of lower specimens were milled with the same machine but under different spindle speeds and feed rates, which not only involved a wide range of technologically applied process in practice, but also produced well finished (highly anisotropic) morphologies [12]. The machining parameters and the corresponding surface roughness parameters are listed in Table 2.

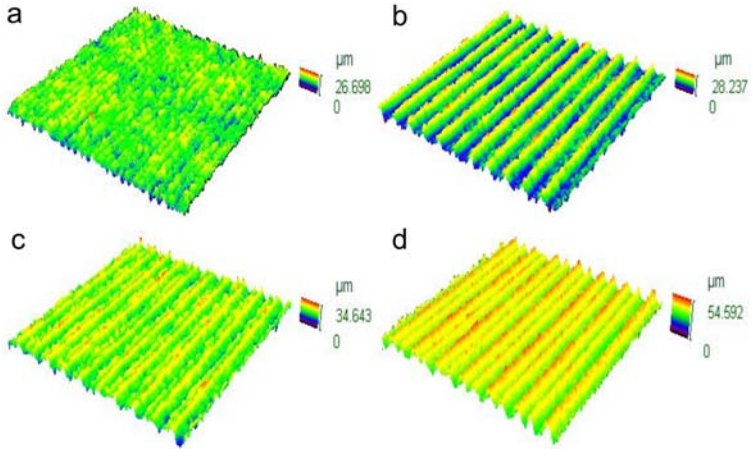

Fig. 3. Typical 3D morphology images of initial surface before tests prepared by milling. (a) S_a=1.737μm ;(b) S_a=3.155μm ;(c) S_a=4.299μm ;(d) S_a=5.261μm.

The initial surface topography of the lower specimens was measured with a 3D optical microscope (OLYMPUS, DSX510). Examples of the 3D topographies are presented in Fig. 3

2.3. Testing methods

In this study, the influence of both surface roughness and texture direction were investigated experimentally. The former was performed by changing the lower specimens which have different initial surface roughness. The latter were performed by changing the relative position between the upper specimen and lower specimen. Specifically, the specimens are first set with the texture parallel to the relative movement direction of the contact interface (Fig. 4(a)), and then the upper specimen was rotated 90°, so that the texture is perpendicular to the relative movement direction of the contact interface (Fig. 4(b)).

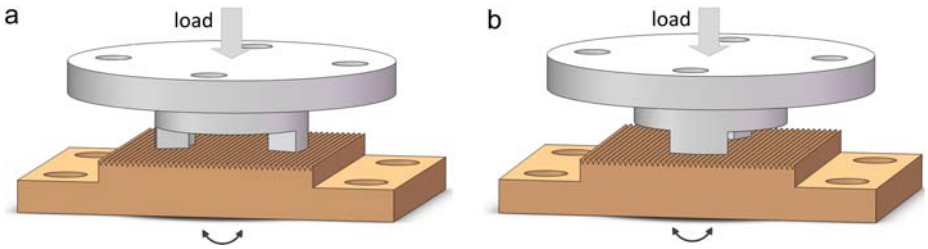

Fig. 4. Fretting wear tests. (a) Texture parallel to the relative movement direction; (b) Texture perpendicular to the relative movement direction.

3. Experimental results and discussion

3.1. Friction torque versus angular displacement amplitude curves

In torsional fretting wear tests, the friction torque versus angular displacement amplitude curves (T-θ curves) provide very important information for fretting wear analysis [26-28]. Firstly, the shape of the T-θ curves reflects the fretting running regime, namely partial slip regime, mixed slip regime or gross slip regime. Secondly, by calculating the amplitude T_i of each T-θ curve, which represents the friction torque of a fretting cycle (as shown in Fig. 5), the friction torque for the whole fretting process can be depicted. Thirdly, the energy dissipated (E_i) for every individual cycle can be calculated by integrating the area of the T-θ curve, and accumulated dissipated energy E_T can be estimated by adding energy dissipated in all cycles.

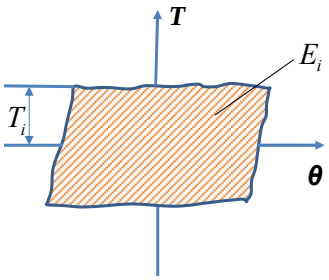

Fig. 5. Friction torque versus angular displacement amplitude curves (T-θ curve).

Fig. 6(a) and (b) display the evolution of *T-θ* curves for texture parallel to the relative movement direction under different surface roughness, while the corresponding curves for texture perpendicular to the relative movement direction are displayed in Fig. 6(c) and (d). All the T-θ curves showed a parallelogram shape, indicating that gross slip occurred between the contact surface and the fretting ran in the gross slip regime, which usually represents serious wear of the contact interface.

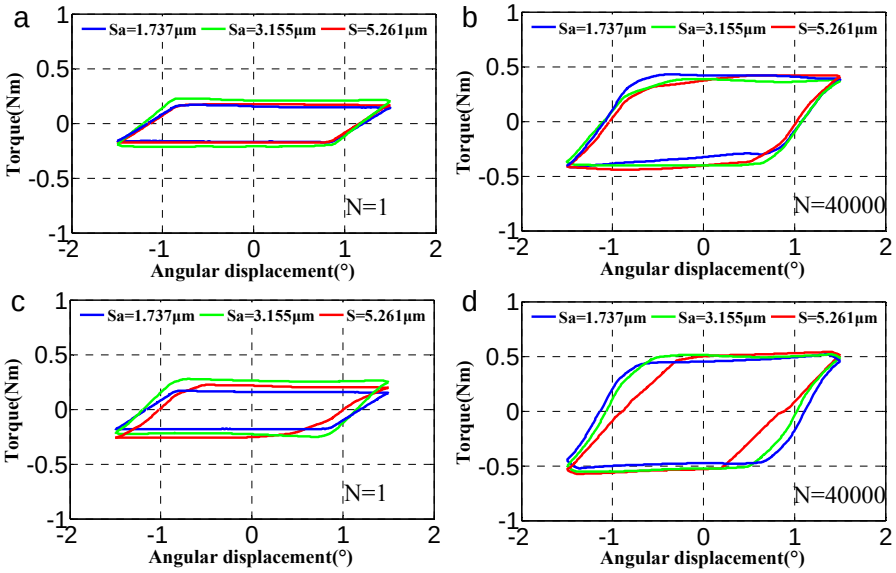

Fig. 6. Typical T-θ curves as a function of number of cycles. (a)(b) With texture parallel to the relative movement direction; (c)(d) With texture perpendicular to the relative movement direction.

3.2. Friction torques

Fig. 7 exhibits the variation of friction torque as a function of number of cycles. From Fig.7 (a) it can be seen that the steady stage friction torques are different at the same texture direction but different initial surface roughness. From Fig. 7(b) it can be seen that the steady stage friction torque are also different at the same roughness but different texture direction. So it proves that both the initial surface roughness and the texture direction have a strong influence on the friction torque.

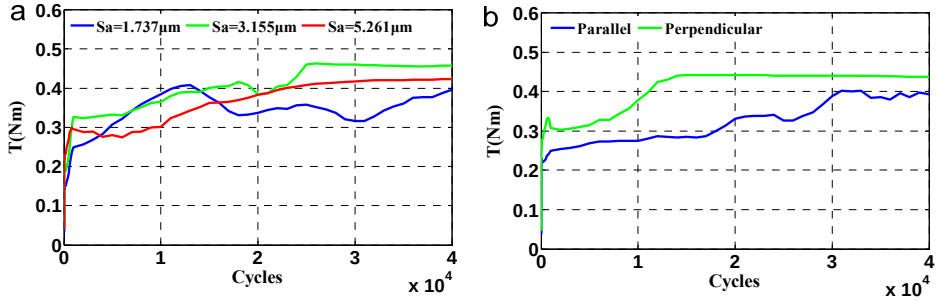

Fig. 7. Friction torques as a number of cycles. (a) Influence of initial surface roughness (parallel to the relative movement direction); (b) Influence of texture direction (S_a=4.553μm).

Dynamic evolution of friction torque during the whole test process is described clearly in Fig. 8, which is plotted with logarithmic coordinates. It can be noted that the friction torque presents lower value in the initial stage due to the protection of the adsorbed and polluted surface films. Then the friction torque climbed in the next few cycles owing to the occurrence of strong plastic deformation in the contact zone. With the third bodies formed and taking part in the fretting process, a balance between the formation and emission of the third bodies was set up, which caused the friction torque to reach the steady stage [23].

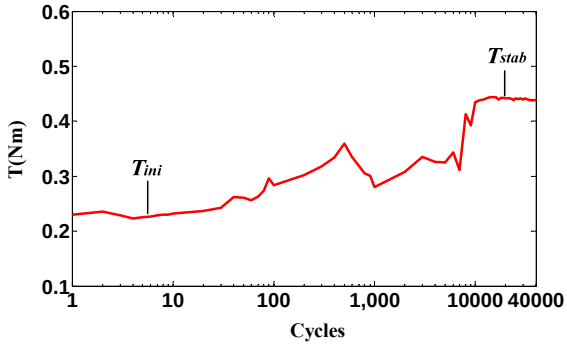

Fig. 8. Typical friction torque under logarithmic coordinate (S_a=4.553μm, parallel to the relative movement direction).

Initial stage friction torque (T_{ini}) and steady stage friction torque (T_{stab}) under different initial surface roughness and texture direction have been calculated and shown in Fig. 9. Note that T_{ini} is defined as the mean value of friction torque for the first 100 cycles and is expressed by

$$T_{ini} = \frac{1}{100}\left[\sum_{1}^{100} T_i\right] \tag{1}$$

While T_{stab} is defined as the mean value of friction torque for the last 10,000 cycles and is expressed by

$$T_{stab} = \frac{1}{10000}\left[\sum_{30000}^{40000} T_i\right] \tag{2}$$

Fig. 9(a) shows that for texture parallel to the relative movement direction, as S_a increases both T_{ini} and T_{stab} show a tendency to first increase and then decrease, peaking at S_a=2.816μm and S_a=3.155μm respectively. Fig. 9(b) shows that when texture is perpendicular to the relative movement direction, as S_a increases, T_{ini} and T_{stab} show a similar tendency to first increase and then decrease, but both of them peak at S_a=3.155μm.

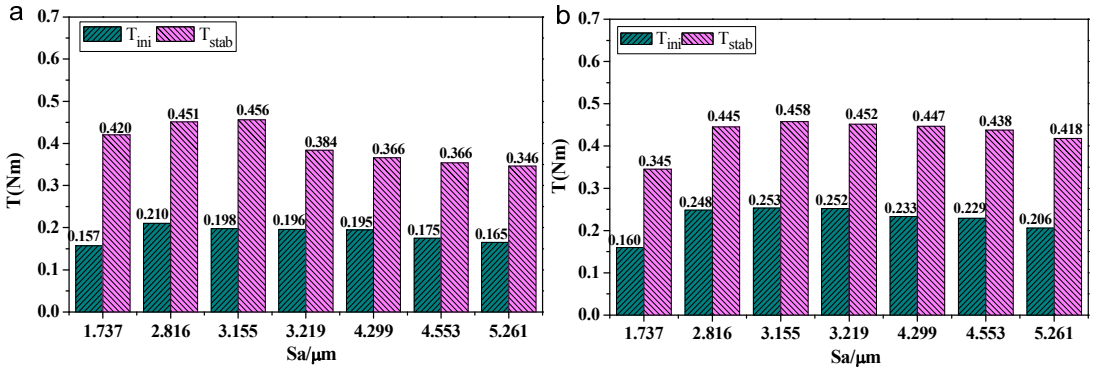

Fig. 9. Initial stage and steady stage friction torque. (a) Parallel to the relative movement direction; (b) Perpendicular to the relative movement direction.

By comparing Fig. 9(a) and (b), the influence of texture direction on T_{ini} and T_{stab} can be studied. It can be seen that under the same S_a, all the T_{ini} values and almost all T_{stab} values are higher when the texture is perpendicular to the relative movement direction; just for S_a=1.737μm and S_a=2.816μm, the T_{stab} values are a little higher for texture parallel to the relative movement direction. Theoretically, a higher value of friction torque can be beneficial in order to prevent transition between partial and gross slip sliding and wear damage mode in industrial components like dovetail, notch, screw joints etc. [14]. Therefore, in engineering applications, to prevent fretting in the gross slip regime and reduce wear, the contact surface needs to be perpendicular to the relative movement direction and with appropriate surface roughness, for example S_a=3.155μm in this study.

3.3. Accumulated dissipated energy

Accumulated dissipated energy (E_T) can be mathematically defined as:

$$E_T = \sum_{i=1}^{n} E_i = \sum_{i=1}^{n} \int_{-\theta}^{\theta} T * \theta d\theta \tag{3}$$

Fig. 10 exhibits the accumulated dissipated energy under different initial surface roughness and texture direction. It can be observed that, for texture parallel and perpendicular to the relative movement direction, with the increase of surface roughness, accumulated dissipated energy also show the tendency to first increase and then decrease, while they peak separately at S_a=2.186μm and S_a=3.219μm. It can also be observed that at the same surface roughness, accumulated dissipated energy is higher when the texture is perpendicular to the relative movement direction; this is mainly because the accumulated dissipated energy is the work of friction torque, and the friction torque is higher when the texture is perpendicular to the relative movement direction (Fig. 9(a) and (b)).

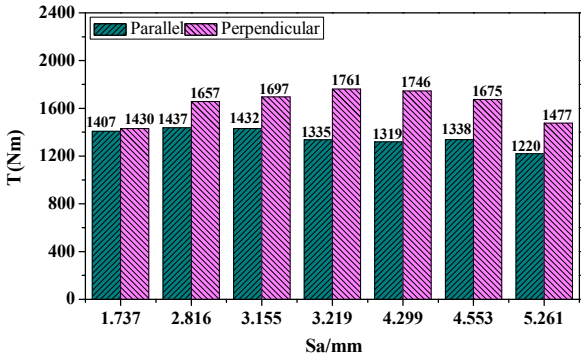

Fig. 10. Influence of surface roughness and texture direction on the accumulated dissipated energy.

3.4. *Wear volume and wear rate*

The wear rate of 42CrMo4 is much lower than CuNiAl [17], so after the tests, mainly the wear of the lower specimen (material, CuNiAl) is considered.

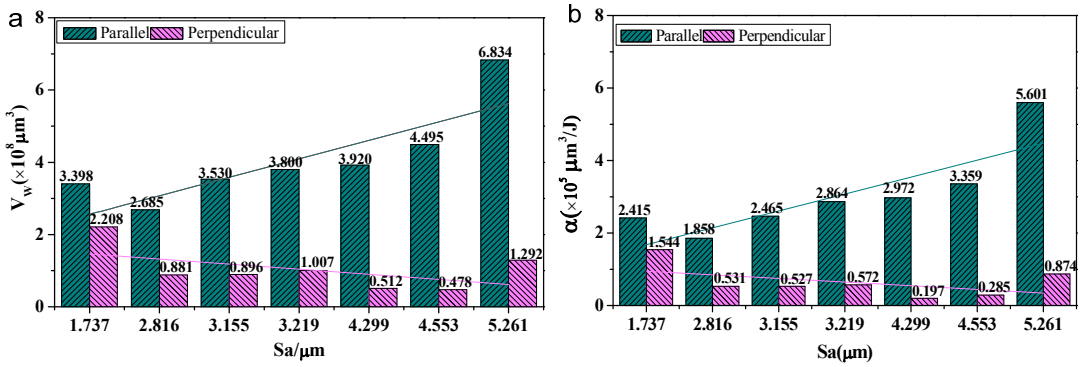

Fig. 11. Influence of surface roughness and texture direction on the wear rate. (a) Wear volume; (b) Wear rate.

Fig. 11(a) shows the wear volume (*Vw*) under different initial surface roughness and texture direction. It can be noted that for texture parallel to the relative movement direction, with the increase of surface roughness, *Vw* decreases from $3.398\times10^8\mu m^3$ to $2.685\times10^8\mu m^3$ at the initial stage, and then steadily increases to $6.834\times10^8\mu m^3$. For the texture perpendicular to the relative movement direction, with the increase of surface roughness, *Vw* firstly shows a decreasing tendency from $2.208\times10^8\mu m^3$ to $0.478\times10^8\mu m^3$, and then increases to $1.292\times10^8\mu m^3$. It is also clear that at the same roughness, the wear volume is much lower for texture perpendicular to the relative movement direction than parallel to it.

Wear rate can be estimated by [29-31]

$$\alpha = \frac{V_w}{E_T} \tag{4}$$

Fig. 11(b) exhibits the wear rate under different initial surface roughness and texture direction. It can be noted that wear rate has the similar change law with wear volume, which can be explained by observing that, as shown in Equation (4), wear rate α is equal to the wear

volume Vw divided by accumulated dissipated energy E_T; as the accumulated dissipated energy E_T varies much less than wear volume Vw (Fig.10 and Fig. 11(a)), the change law of wear rate α is in highly accordance with wear rate Vw. From Fig. 11, it is also clear that the wear volume and wear rate are highly affected by the texture direction, and they are much lower when the texture is perpendicular to the relative movement direction.

The above analysis reveals that by proper initial surface topography control and modification, wear of the contact interface can be reduced, which is useful for extending the lifetime of the elements in engineering applications.

4. Conclusions

The influence of surface roughness and texture direction on fretting wear behavior was experimentally investigated with a flat-on-flat contact test rig. From analysis of the results the following conclusions can be obtained:

(1) Initial surface roughness and texture direction have a great influence on the fretting wear rate.

(2) With the increase of surface roughness, both friction torque and accumulated dissipated energy present the tendency to first increase and then decrease, and their value tend to be higher when texture is perpendicular to the relative movement direction.

(3) For texture parallel to the relative movement direction, wear volume and wear rate present increasing tendency as the surface roughness increase; for texture perpendicular to the relative movement direction, wear volume and wear rate present decreasing tendency as the surface roughness increase.

(4) Wear rate are lower when the texture is perpendicular to the relative movement direction.

Acknowledgements

This work was supported by the National Natural Science Foundation of China (Grant Nos. 51475192, 51475190), National Basic Research Program of China (2014CB046705).

References

[1] Golchin A, Friedrich K, Noll A, et al. Influence of counter surface topography on the tribological behavior of carbon-filled PPS composites in water. Tribology International 2015; 88:209-217.

[2] Timma C, Lostak T, Janssen S, et al. Surface investigation and tribological mechanism

of a sulfate-based lubricant deposited on zinc-coated steel sheets. Applied Surface Science 2016; 390: 784-794.

[3] Zhang HY, Blunt LA, Jiang XQ, et al. The influence of bone cement type on production of fretting wear on the femoral stem surface. Clinical Biomechanics 2012; 27:666-72.

[4] Ghosh A, Sadeghi F. A novel approach to model effects of surface roughness parameters on wear. Wear 2015; 338:73-94.

[5] Zhang HY, Luo JB, Zhou M, et al. Biotribological properties at the stem–cement interface lubricated with different media. Journal of the Mechanical Behavior of Biomedical Materials 2013; 20:209-16.

[6] Blunt LA, Zhang HY, Barrans SM, et al. What results in fretting wear on polished femoral stems. Tribology International 2009; 42:1605-14.

[7] Arnholt C, Underwood R, MacDonald D, et al. Microgrooved Surface Topography Does Not Influence Fretting Corrosion of Tapers in Total Hip Arthroplasty: Classification and Retrieval Analysis: Modularity and Tapers in Total Joint Replacement Devices. ASTM International, 2015.

[8] Xiong DS, Qin YK, Li JL, et al. Tribological properties of PTFE/laser surface textured stainless steel under starved oil lubrication. Tribology International, 2015, 82: 305-310.

[9] Ceschini L, Martini C, Morri A. Dry sliding wear of an induction-hardened, high-silicon medium-carbon microalloyed steel. Tribology International, 2015; 92: 493-502.

[10] Zhu Y, Chen X, Zou J, et al. A study on the influence of surface topography on the low-speed tribological performance of port plates in axial piston pumps. Wear 2015; 338:406-17.

[11] Wyatt H, Elliott M, Revill P, et al. The effect of engineered surface topography on the tribology of CFR-PEEK for novel hip implant materials. Biotribology 2016; 7:22-30.

[12] Kubiak KJ, Mathia TG. Influence of roughness on contact interface in fretting under dry and boundary lubricated sliding regimes. Wear 2009; 267:315-21.

[13] Kubiak KJ, Bigerelle M, Mathia TG, et al. Dynamic evolution of interface roughness during friction and wear processes. Scanning 2014; 36:30-8.

[14] Kubiak KJ, Liskiewicz TW, Mathia TG. Surface morphology in engineering applications: Influence of roughness on sliding and wear in dry fretting. Tribology International 2011; 44:1427-32.

[15] Kubiak KJ, Mathia TG, Fouvry S. Interface roughness effect on friction map under fretting contact conditions. Tribology International 2010; 43:1500-7.

[16] Pawlus P, Michalczewski R, Lenart A, et al. The effect of random surface topography height on fretting in dry gross slip conditions. Proceedings of the Institution of Mechanical Engineers, Part J: Journal of Engineering Tribology 2014; 228:1374-91.

[17] Godjevac M. Wear and friction in a controllable pitch propeller. Doctoral dissertation,

TU Delft, Delft University of Technology, 2010.

[18] Wang SB, Teng B, Zhang S. Torsional wear behavior of monomer casting nylon composites reinforced with GF: effect of content of glass fiber. Tribology Transactions 2013; 56:178-86.

[19] Zhang X, Shen HM, Liu J, et al. An efficient numerical model for predicting the torsional fretting wear considering real rough surface. Wear 2015; 344:32-45.

[20] Yang J, Mo JL, Cai ZB, et al. Identification between rotational fretting and rotational wear of PMMA/steel by means of tribo-noise and tribo-vibration signals. Tribology International 2013; 59:1-9.

[21] Shen MX, Cai ZB, Peng JF, et al. Dual-rotary fretting wear of 7075 alloy in media of oil and water. Wear 2013; 301:540-50.

[22] Hintikka J, Lehtovaara A, Mäntylä A. Fretting-induced friction and wear in large flat-on-flat contact with quenched and tempered steel. Tribology International, 2015, 92: 191-202.

[23] Mi X, Wang WX, Xiong XM, et al. Investigation of fretting wear behavior of Inconel 690 alloy in tube/plate contact configuration. Wear, 2015, 328: 582-590.

[24] Leonard BD. An experimental and numerical investigation of the effect of coatings and the third body on fretting wear. Doctoral dissertation, Purdue University, 2012.

[25] Leonard BD, Patil P, Slack TS, et al. Fretting wear modeling of coated and uncoated surfaces using the combined finite-discrete element method. Journal of Tribology 2011; 133: 021601.

[26] Quan H, Gao S, Zhu M, et al. Comparison of the torsional fretting behavior of three porous titanium coatings for biomedical applications. Tribology International, 2015; 92: 29-37.

[27] Wang S, Wang F, Liao Z, et al. Study on torsional fretting wear behavior of a ball-on-socket contact configuration simulating an artificial cervical disk. Materials Science and Engineering: C, 2015; 55: 22-33.

[28] Cai ZB, Shen MX, Yu J, et al. Friction and wear behavior of UHMWPE against titanium alloy ball and alumina femoral head due to torsional fretting. International Journal of Surface Science and Engineering, 2013; 7: 81-95.

[29] Haviez L, Fouvry S, Toscano R, et al. An energy-based approach to understand the effect of fretting displacement amplitude on grease-lubricated interface. Wear, 2015, 338: 422-429.

[30] Alarcón G I, Burgelman N, Meza JM, et al. The influence of rail lubrication on energy dissipation in the wheel/rail contact: a comparison of simulation results with field measurements. Wear, 2015; 330: 533-539.

[31] Berthel B, Moustafa A R, Charkaluk E, et al. Crack nucleation threshold under fretting

loading by a thermal method. Tribology International, 2014, 76: 35-44.